© 2016. Published by The Company of Biologists Ltd | Journal of Cell Science (2016) 129, 3462-3472 doi:10.1242/jcs.191148

RESEARCH ARTICLE

Local Ras activation, PTEN pattern, and global actin flow in the chemotactic responses of oversized cells

Markus Lange[1], Jana Prassler[1], Mary Ecke[1], Annette Müller-Taubenberger[2] and Günther Gerisch[1,*]

ABSTRACT

Chemotactic responses of eukaryotic cells require a signal processing system that translates an external gradient of attractant into directed motion. To challenge the response system to its limits, we increased the size of *Dictyostelium discoideum* cells by using electric-pulse-induced fusion. Large cells formed multiple protrusions at different sites along the gradient of chemoattractant, independently turned towards the gradient and competed with each other. Finally, these cells succeeded to re-establish polarity by coordinating front and tail activities. To analyse the responses, we combined two approaches, one aimed at local responses by visualising the dynamics of Ras activation at the front regions of reorientating cells, the other at global changes of polarity by monitoring front-to-tail-directed actin flow. Asymmetric Ras activation in turning protrusions underscores that gradients can be sensed locally and translated into orientation. Different to cells of normal size, the polarity of large cells is not linked to an increasing front-to-tail gradient of the PIP3-phosphatase PTEN. But even in large cells, the front communicates with the tail through an actin flow that might act as carrier of a protrusion inhibitor.

KEY WORDS: Actin flow, Cell fusion, Cell polarity, Chemotaxis, PTEN, Ras

INTRODUCTION

Orientation of eukaryotic cells in a gradient of chemoattractant requires a signal processing system that translates an external gradient of signalling molecules, recognised by receptors on the cell surface, into a directed motion based on the polarisation of cytoskeletal activities. Models of chemotaxis emphasize either a global view or focus on local responses. The global aspect of front-to-tail polarisation has been addressed in the reaction-diffusion model of Meinhardt and Gierer (2000), and in various versions of the local excitation global inhibition (LEGI) model (Iglesias and Devreotes, 2008). Local aspects are underlined in pseudopod-based models as the split-pseudopod model of Insall (Insall, 2010) or the local coupling model of Arrieumerlou and Meyer (2005).

Our goal was to challenge the response system by increasing its size. A large cell needs to coordinate local activities over long distances, in order to reorientate when the direction of a gradient is changing. Using electric-pulse-induced fusion we produced large cells of *Dictyostelium discoideum* (Gerisch et al., 2013) and allowed them to align in a gradient of attractant. Subsequently, the cells were forced to reorientate by moving a stimulating micropipette behind their tails. To analyse the responses of these cells, we combined two approaches, one aimed at local activities, the other at global responses. Local activities were recorded by visualising the dynamics of Ras activation at protrusions formed during reorientation of the cells. The large cells formed multiple protrusions that, independently, turned into the direction of the gradient. Asymmetric Ras activation across the diameter of the tubular protrusions indicates that the gradient is locally sensed and translated into a response.

In global terms, the reorientation of oversized cells is characterised by the conflict between persistent cell polarity and the reversed direction of an attractant gradient. In this conflict, the response was often initiated opposite to the source of attractant: protrusions were first formed at the previous front – at sites of lowest attractant concentration – and only subsequently at the previous tail, which received the strongest attractant signal. To monitor how a response governed by the intrinsic polarity of the cell is converted into a response directed by the external gradient, we used a Ras-binding domain (RBD) as a front marker (Zhang et al., 2008). The RBD of human Raf1 recognizes the GTP-bound state of Ras G (Kae et al., 2007), which is important for chemotaxis in *Dictyostelium* (Takeda et al., 2012).

The recording of activated Ras was combined with that of membrane-bound PTEN. In chemotaxing cells of normal size, the binding of this PI3-phosphatase to the inner face of the plasma membrane has been reported to increase from the front to the tail (Funamoto et al., 2002; Iijima and Devreotes, 2002). The question was whether this gradient can accommodate to an enlarged cellular space. Quantitative fluorescence imaging revealed that, on the substrate-attached surface of large cells, PTEN reached a peak behind the front and then declined until reaching the tail; it thus did not reflect the polarity of the cell.

As an alternative mechanism of front-to-tail coordination, we explored the possibility of a directed actin flow. In normal-sized *Dictyostelium* cells that expressed a talin fragment as an actin-binding probe, an actin flow directed from high to low attractant concentrations has been demonstrated previously (Weber et al., 2002). By simultaneously recording Ras activation and direction of the actin flow, we show here that, even over the increased distances of a large cell, a global actin flow connects the front with the tail, and the flow is redirected when the attractant gradient is changed. This finding prompted us to discuss the possibility that the front-to-tail polarity in the chemotactic response is established through molecules carried by a flow of actin and specify the tail of the cell.

RESULTS

Chemotaxis of large cells

Under stationary chemotactic stimulation, a cell moves with its axis of polarity pointing towards the concentration gradient of

[1]Max Planck Institute of Biochemistry, Am Klopferspitz 18, Martinsried D-82152, Germany. [2]LMU Munich, Department of Cell Biology (Anatomy III), BioMedical Center, Großhaderner Str. 9, Martinsried D-82152, Germany.

*Author for correspondence (gerisch@biochem.mpg.de)

G.G., 0000-0002-8348-1924

Received 18 April 2016; Accepted 1 August 2016

Journal of Cell Science (2016) 129, 3462-3472 doi:10.1242/jcs.191148

chemoattractant. To study how a large cell responds if its polarity and the attractant gradient point into opposite directions, fused cells of *Dictyostelium* were stimulated with cAMP through a micropipette, allowing them to align their polarity with the gradient, and then suddenly reverted the gradient direction by moving the pipette. To trace changes in cell polarisation, we used cells in which the mRFP-tagged Ras-binding domain (RBD) from human Raf1 was expressed as a front marker (Zhang et al., 2008). This front marker was combined with GFP-tagged PTEN. In a chemotaxing cell of normal size, binding of this PI3-phosphatase to the inner face of the plasma membrane is considered to rise from the front to the tail (Funamoto et al., 2002; Iijima and Devreotes, 2002).

Multifold increases of cell size following electric-pulse-induced fusion are illustrated in Fig. 1A and Movie 1, where a cell of normal size and two large ones respond concomitantly to attractant gradients of changing directions. In Fig. 1B-D, quantitative data on the chemotactic response of a cell five times larger than normal are presented. The large cell was forced to repeatedly reorientate in response to changing positions of a micropipette (Fig. 1B), and its velocity in terms of the centroid displacement was measured. In moving towards a stationary micropipette, the cell had an average velocity of 0.116 µm s^{-1}±0.016 (mean±s.e.m.) (Fig. 1C). This means, the large cell was slower than normal-sized cells, for which a velocity of 0.253 µm s^{-1}±0.022 (mean±s.e.m.) was obtained as an average of ten cells orientated in a cAMP gradient under the same conditions.

For the same large cell, a chemotactic index was calculated from the cosine of α, the angle between the direction of centroid displacement and the direction of the micropipette tip. The chemotactic index can vary between 0 and +1 for positive chemotaxis and between 0 and −1 for negative chemotaxis. During cell movement towards stable micropipette positions, an average value as high as a chemotactic index=0.912±0.036 (mean±s.e.m.) was reached, indicating efficient orientation of the large cell in the gradient (Fig. 1D). Upon changing the position of the micropipette, the chemotactic index became temporarily negative because the cell continued to move in the previous direction. However, the recovery of the chemotactic index to positive values indicates reorientation of the large cell in 61 s or less, as indicated in Fig. 1D. Since this time comprises the reversal of the diffusion gradient and the response of the cell to the reversed gradient, it is an upper limit for reorientation of the large cell.

Strategies to reorientate

Upon the sudden reversal of the external gradient, the established front of the cell still pointed into the direction of the previous gradient, such that the attractant preferentially hit the tail region of the cell. To readjust their polarity to the new direction of the

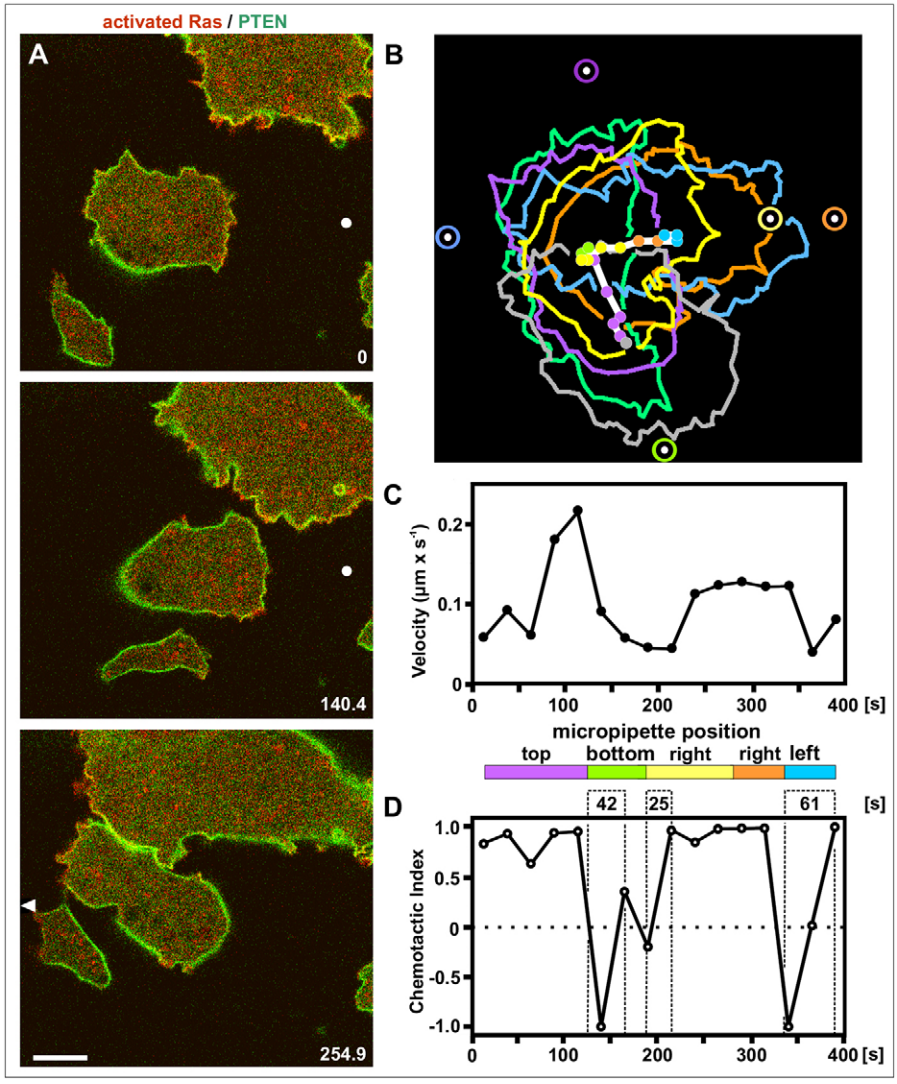

Fig. 1. Chemotactic reorientation of large cells in diffusion gradients of cAMP. (A) Three cells of different sizes responding to a micropipette filled with the attractant. The micropipette was moved from the right to the left. Its tip position is indicated by a dot if the tip is located within the frame, or by an arrowhead pointing towards a position outside the frame. The cells expressing mRFP-RBD to label activated Ras (red) and PTEN-GFP (green) illustrate size variations in a population subjected to electric-pulse-induced fusion. The small cell on the bottom is probably uninucleate. The confocal cross-sections through the cells are focused to a plane 1.5 µm beyond the substrate surface. Time is indicated in seconds after the first frame. The entire time series is shown in Movie 1. (B) Tracking a large cell that reorientates in response to changing micropipette positions. The area covered by the cell was 689 $µm^2$, as compared to 142 $µm^2$±10 (mean±s.e.m.), the area obtained from 10 non-fused control cells responding to cAMP gradients under the same conditions. Cell contours at different times are colour-coded corresponding to changing micropipette positions, which are indicated by white dots within coloured circles. The cell contour at the beginning of the sequence is displayed in grey. Centroid positions are plotted at intervals of 8.6 s as coloured dots that are connected by a bold white line. (C) Velocities of centroid displacement of the cell shown in B. The colour bar indicates phases of micropipette position in accord with the colour code in B. (D) Chemotactic index calculated from displacement of the centroid. Numbers between dotted lines indicate delays in seconds of reorientation after moving the micropipette. Scale bars: 10 µm (A). Frame size of B: 68 µm x 68 µm.

Journal of Cell Science (2016) 129, 3462-3472 doi:10.1242/jcs.191148

gradient, the large cells employed a variety of strategies. In one type of response, cell polarity was controlled by the external gradient of chemoattractant. The cells reversed their polarity as a whole, converting the previous front into a tail and vice versa. However, in the majority of responses, the established polarity of the cells influenced the way they reorientated. The variability of responses in a single cell is illustrated in Movie 2, where a cell reorientated first by reverting its polarity and, after repositioning the micropipette, by forming multiple protrusions.

Three characteristic examples of reorientation are illustrated in Fig. 2. These images highlight activated Ras (red), together with membrane-bound PTEN (green) against a low cytoplasmic background of unbound PTEN. The cell depicted in Fig. 2A and Movie 3 shows the turning of a lateral protrusion combined with asymmetric Ras activation at the side exposed to the higher attractant concentration. The relatively small cell of Fig. 2B and Movie 4 had two fronts marked by activated Ras. One front turned into a tail, whereas the other branched and continued to protrude. Notably, it was the front closest to the source of attractant that became inhibited and converted into the tail. Upon moving the micropipette, this tail finally turned into a new front, suppressing other protrusions. The cell in Fig. 2C and Movie 5 initially formed a protrusion that emanated from its established front. This protrusion turned into the direction of the new gradient, until a lateral protrusion dominated the response and became the new leading edge. In its orientation towards the source of attractant, this protrusion showed a split-pseudopod behaviour as described for the chemotactic orientation of *Dictyostelium* cells (Andrew and Insall, 2007) and also for their unbiased movement (Bosgraaf and Van Haastert, 2009). These three image series indicate that protrusions are induced at multiple sites along the surface of large cells and not only at regions of highest attractant concentration. Irrespective of the site of their induction, protrusions recognize the new gradient and turn into its direction, indicating that turning of the protrusions is a response to the gradient that is separate from their induction.

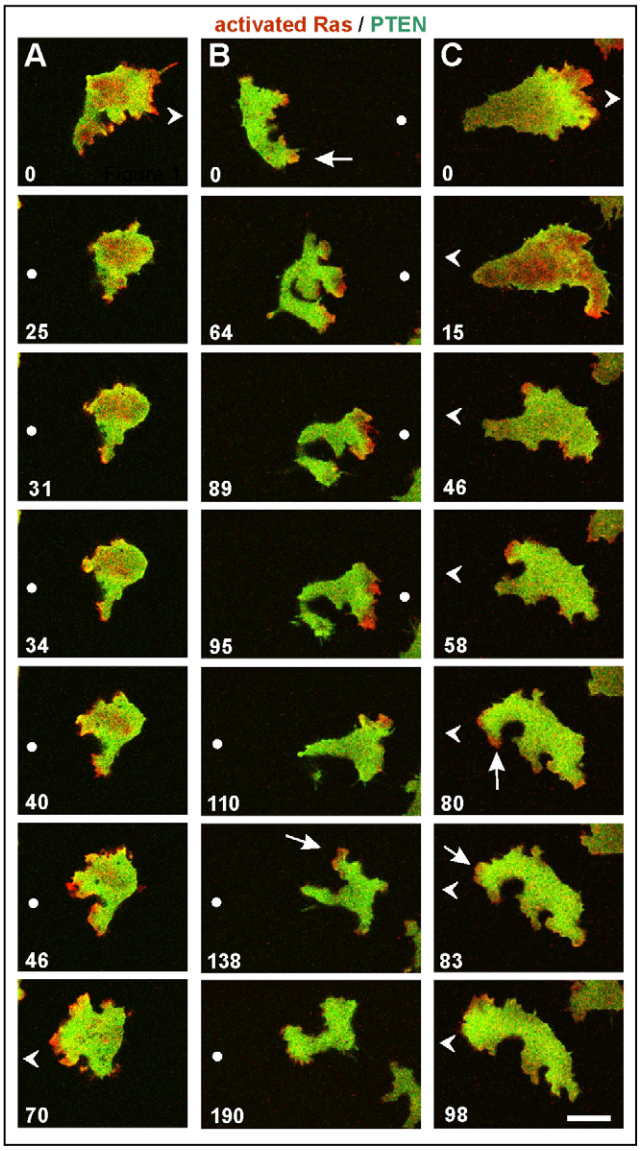

Fig. 2. Overview on the chemotactic responses of large cells. Images of reorientating cells are focused on the plane of the substrate-attached membrane. The cells expressed mRFP-RBD to label activated Ras (red) and PTEN-GFP (green). The tip position of the micropipette is indicated by a dot if the tip is located within the frame or by an arrowhead pointing towards a position outside the frame. (A) At the beginning, the cell is orientated towards the source of the gradient with a broad front and with a branched protrusion emerging from the tail region. After repositioning the micropipette, a lateral protrusion expands normal to the direction of the new gradient, until a new front pointing into the direction of the gradient is established. (B) This cell forms two fronts, before the front that had been closest to the source of attractant turns into a tail. Upon reorientation, this tail is converted into a front that competes successfully with the previous front. Asymmetric Ras activation is indicated by an arrow in the 138-s frame. (C) The first images illustrate a protrusion emerging from the previous front region, which turns into the direction of the gradient and finally converts into the tail of the reorientated cell. Thereafter, a lateral protrusion takes over the lead and guides the cell up the gradient. Arrows in the 80-s and 83-s frames point to split-pseudopodia formation. Scale bar: 10 µm. The cells displayed in A–C are also shown in Movies 3–5.

Dual-front movement

Taken together, of the 66 large cells tracked during reorientation, 23 cells transiently responded by forming two protrusions, 11 cells formed multiple fronts and 32 cells formed single, often broad and subdivided fronts. The responses of cells forming two protruding fronts were analysed in detail. How do these two fronts cooperate in driving the cell body towards the source of attractant and, also, compete with each other, such that eventually one front maintains the anterior position, while the other that is being retracted may turn into a tail? In Fig. 3 and Movie 6, movement and shape changes are represented at intervals of about 9 s by indicating the gain of area covered by the cell body (red) and the loss of area (blue). The three cells shown illustrate various features of the interplay of protrusion and retraction. In Fig. 3A, the bifurcation of the cell into two lobes develops from a state with multiple protrusions (0-s to 101.0-s, and 165.2-s to 192.8-s frames during reorientation). In the first period, the two fronts coexist for more than 95 s before one of them starts to retract (45.9-s to 101.0-s frames). The cell in Fig. 3B and Movie 6 shows the formation of two protrusions that are separated by a retracting zone (18.4-s and 27.5-s frames). Subsequently, the protrusions merge into one broad front, while the retracting zone between them disappears (36.7-s to 64.3-s frames). In the cell shown in Fig. 3C and Movie 6, protrusive activities progress from the previous front region towards the previous tail. Simultaneously, the cell retracts until two fronts are formed that protrude into the direction of the gradient.

Tracking the centroid of the cells enabled us to relate the velocity of centroid displacement and the chemotactic index to the balance of protrusions and retractions (Fig. 3D to I). When the cell of Fig. 3A switched from movement with two fronts to movement

Journal of Cell Science (2016) 129, 3462-3472 doi:10.1242/jcs.191148

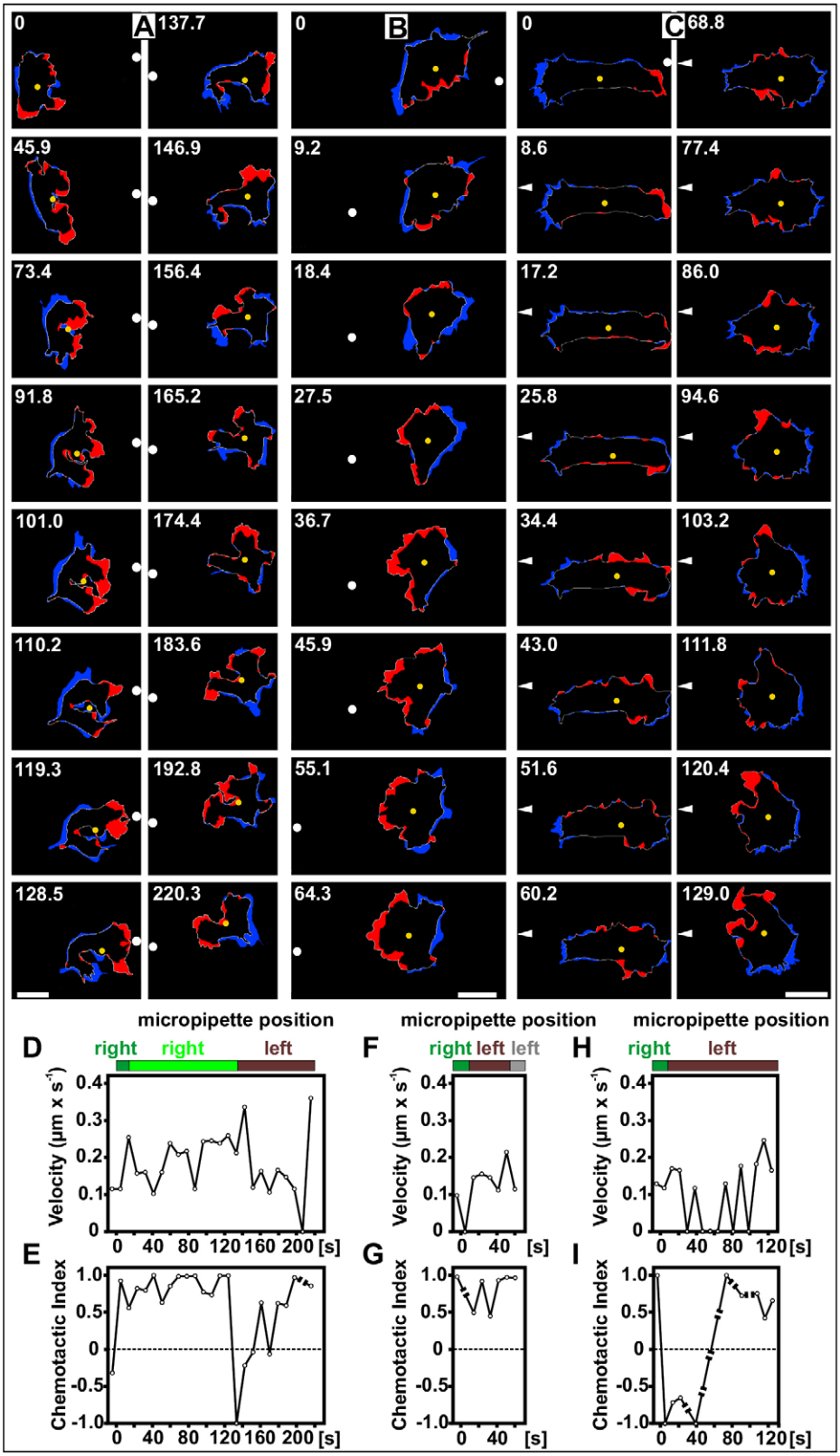

Fig. 3. Gain (red) and loss (blue) of cell area in large cells responding to reversal of an attractant gradient. (A–C) Three cells that reorientate by protruding two fronts. The tip position of the micropipette is indicated by a dot if the tip is located within the frame or by an arrowhead pointing towards a position outside the frame; centroid positions are yellow dots. Time after the first frame of each series is indicated in seconds. The gain and loss of area represents the changes in cell shape and position between two frames recorded at intervals of 9.2 s (A,B) or 8.6 s (C). The cell in C is also shown in Movie 2. Scale bars: 10 µm. (D,F,H) Velocities based on centroid displacements in the three cells shown in A–C, respectively. (E,G,I) Chemotactic indices derived from centroid displacements corresponding to D–F, respectively. Gain and loss in the three cells displayed in A–C are also shown in Movie 6.

with one front between the 101.0-s and the 128.5-s frame, no obvious change of velocity occurred because the fast protrusion of the remaining front compensated for any retraction (Fig. 3D). At a later switch, net movement stopped briefly at 206 s when one front was retracted. In this cell, a high chemotactic index was reached during the initial period of continuous dual-front progression (Fig. 3E). During this period, an average chemotactic index of 0.857±0.041 (mean±s.e.m.) was obtained from the centroid displacements measured over ten frame-to-frame intervals.

Journal of Cell Science (2016) 129, 3462-3472 doi:10.1242/jcs.191148

The cell shown in Fig. 3B stopped net movement at 5 s upon repositioning of the micropipette (Fig. 3F) but continued to form protrusions and to retract locally (18.4-s frame in Fig. 3B). Subsequently, the cell moved again – well-orientated in the attractant gradient (Fig. 3G) – while its two protrusions fused into one (36.7-s to 64.3-s frames in Fig. 3B).

Fig. 3C exemplifies a cell that needed longer than the previous ones to reorientate but eventually responded efficiently to the changed gradient, as shown in Movie 2. In a first phase, the cell formed protrusions near the previous front. However, retraction of the previous tail shifted the centroid away from the source of attractant, such that the chemotactic index became negative (Fig. 3I). In an interphase from about 50–110 s, protrusive and retractive activities brought net movement repeatedly to a halt (Fig. 3H) before the cell moved with two protrusions efficiently towards the micropipette.

The gain of area as a measure of the local protrusion rate can be compared with the centroid displacement reflecting global translocation of the cell mass. As shown in Table 1, local protrusions reached velocities that are about three times higher than the corresponding centroid displacements.

In summary, dual-front movement is compatible with effective chemotactic orientation. Details of the interplay of local protrusions and retractions in a reorientating large cell are, however, not reflected in the chemotactic index based on displacement of the centroid.

Asymmetric Ras activation in turning protrusions

Given that the chemotactic response of the cell shown in Fig. 2A suggested a link between turning and the asymmetric activation of Ras, we located activated Ras in optical sections across turning protrusions. The time series of Fig. 4 shows the local evolution of asymmetric Ras distribution within a protrusion that turned towards a gradient of attractant as compared to changes in PTEN distribution. Comparison of the 24.5-s to 27.5-s frames reveals that Ras was already activated at the membrane area proximal to the micropipette before PTEN had disappeared. After the asymmetric activation of Ras, PTEN declined within that area to levels below those within the opposite distal membrane region (27.5-s frame and following ones).

A special case of membrane dynamics in a protrusion is displayed in Fig. 5. While turning into the direction of the gradient, the membrane area decorated with activated Ras was endocytosed in two events of macropinocytosis, indicating that protrusion and turning is compatible with the internalisation of membrane. This finding underlines the dynamics of Ras activation, indicating that the attractant-induced pattern of activated Ras on a new membrane area is restored within 5 s.

The localised control of Ras activation is underlined by the fact that Ras can be activated simultaneously at the front of a large cell that points in the direction of an attractant gradient and in the form of circular waves that propagate on the substrate-attached surface. It has previously been observed that cells of the *Dictyostelium* AX2 strain form actin waves, which circumscribe a membrane territory that is rich in PIP3. This inner territory is separated from an outer PTEN-decorated area (Arai et al., 2010; Gerisch et al., 2012). The

Table 1. Maximal velocities of protrusions compared to centroid displacements

Cell and frame in Fig. 3		Velocity of protrusion [μm s^{-1}]	Displacement of centroid [μm s^{-1}]
A	119.3 s	0.67	0.24
B	64.3 s	0.38	0.12
C	120.4 s	0.50	0.18

In each of the three image series of Fig. 3, the maximal rate of local protrusion was scored and related to displacement of the cell's centroid within the same interval in time.

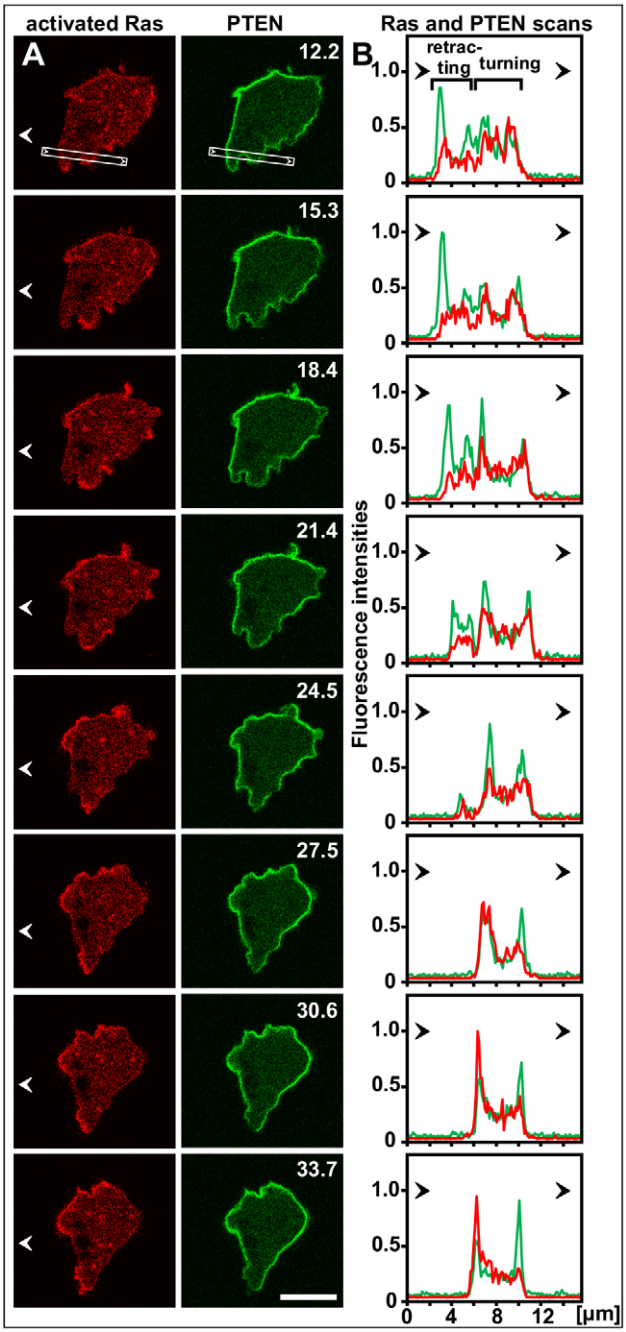

Fig. 4. Asymmetric Ras activation and membrane-bound PTEN pattern in the protrusion of a large cell that turns into the direction of an attractant gradient. The same cell as in Fig. 2A is shown expressing mRFP-RBD and PTEN-GFP. (A) Optical cross-sections through the protrusion at 1.5 μm above the substrate surface, showing mRFP-RBD images in the left panels, and PTEN-GFP images in the right panels. (B) Scans of fluorescence intensities across the turning protrusion along the bar shown in the first panel in A. The scan direction (arrowheads) is adjusted to the position of the micropipette at the left of the scans. Up to the 24.5-s frame, the scan crosses two protrusions, the left one does not show asymmetric Ras activation and is retracting (indicated by brackets in the 12.2-s frame). Time is indicated in seconds; the 12.2-s image has been acquired at 3 s after positioning the micropipette to the left of the frame. The 24.5-s image corresponds to the 25-s image in Fig. 2A. Scale bar: 10 μm. Six turning protrusions analysed showed similar patterns of asymmetry.

Journal of Cell Science (2016) 129, 3462-3472 doi:10.1242/jcs.191148

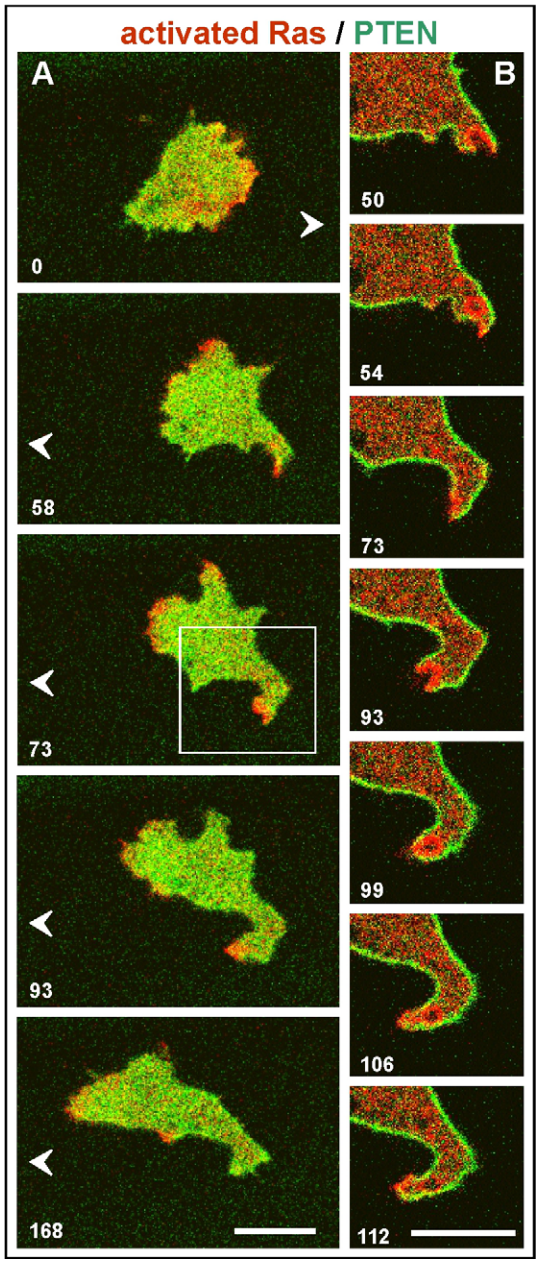

Fig. 5. A cell with a protrusion undergoing macropinocytosis during turning. (A) Merged RBD and PTEN images focused close to the substrate surface, showing asymmetric Ras activation in the 73-s frame between two events of macropinocytosis. (B) Merged images of the area framed in the 73-s image of A, focused to 1.5 µm above the substrate surface. Time is indicated in seconds. Scale bars: 10 µm. The tip position of the micropipette is indicated by an arrowhead pointing towards a position outside the frame.

inner territory is also distinguished by the activation of Ras (Huang et al., 2013). Movie 7 shows a very large cell to demonstrate that wave formation and chemotaxis do not exclude each other; activation of Ras within large territories coincides with the chemotactic response within another part of the cell.

PTEN dynamics in large cells that respond to changing gradients

Membrane-bound PTEN has been reported to be reduced at the front of chemotaxing cells and to be highest at their tail regions (Funamoto et al., 2002; Iijima and Devreotes, 2002). Therefore, we asked whether – in enlarged cells – PTEN binding continues to increase along the entire front-to-tail axis of the cells. To obtain comprehensive information on the pattern of PTEN, we determined its distribution within two planes of focus: (1) in the plane of the substrate-attached membrane and (2) in a cross-section through the free membrane 1.5 µm above the substrate-attached surface.

The double-view imaging revealed two different patterns of PTEN distribution in chemotaxing cells. At the substrate-attached membrane, PTEN showed a characteristic enrichment within the anterior zone (Fig. 6A-C). The posterior region of the cell became almost depleted of PTEN; nevertheless, formation of pseudopods was suppressed in this region. Upon chemotactic reorientation, this PTEN pattern was re-established within less than 40 s of exposing a cell to a new direction of the gradient. The change in the PTEN pattern requires an increase in membrane binding near to the new front zone and a decrease in the previous front region. The decrease proceeded as previously reported for the PTEN regulation in actin waves (Gerisch et al., 2012). PTEN was downregulated through localised depletion, often resulting in the formation of 'PTEN holes' before the typical enrichment of PTEN at the new anterior region of the cell was re-established (Fig. 6D and Movie 8, left panel).

In cross-sections through the cell at 1.5 µm above the substrate-attached surface, activated Ras located in protrusions, and PTEN strongly decorated the membrane up to the tail region (Fig. 6E and Movie 8, right panel). At an early stage after changing the gradient direction, the protrusions were distributed over most of the cell surface (0-s, 188-s, 219-s and 401-s frames of Fig. 6E). At later stages, the large cells clearly became polarised, with less patches of activated Ras at the tail region (88-s and 299-s frames). In these polarised states, the fluorescence intensity of GFP-PTEN was scanned in the cross-sections along the perimeter of the cell, beginning with the front and ending with the tail (Fig. 6F). The scans did not show an increase of PTEN decoration from the front to the tail, although the tail appeared to be more uniformly decorated than the front region.

Redirected actin flow during establishment of polarity

The absence of a continuous PTEN gradient has prompted us to search for other mechanisms of coordinated front and tail establishment in large cells. Since previous work on normal-sized cells revealed a retrograde actin flow in chemotaxing *Dictyostelium* cells (Weber et al., 2002), we asked whether a continuous flow would connect front and tail along the entire length of a fused cell. A GFP-fusion of the C-terminal actin-binding domain of talinA (GFP-talC63) has been shown to be transported with the flow and, because of its slow dissociation, to accumulate at the tail of the cell (Weber et al., 2002). To simultaneously monitor actin flow and changes in polarity, we used cells that express the flow reporter (green) together with mRFP-RBD as a front marker (red). Fig. 7 illustrates how, in large cells, changes in polarity upon chemotactic reorientation are reflected in altered directions of the flow. In Fig. 7A and Movie 9 the position of the micropipette was changed twice. In the first phase (frames 72-s to 108-s of Movie 9), multiple protrusions identified by Ras activation were induced. The actin flow was directed away from these protrusions, which competed with each other. In the second phase (frames 108-s to 260-s of the movie), a new front opposite to the previous one was established, and the actin flow was reversed accordingly.

Fig. 7B and Movie 10 show a tail region established in the middle of a large cell, at the junction between two or three front zones. Finally, Fig. 7C and Movie 11 display a complex response in which the modes of reorientation shown in Fig. 7A,B were combined with

Journal of Cell Science (2016) 129, 3462-3472 doi:10.1242/jcs.191148

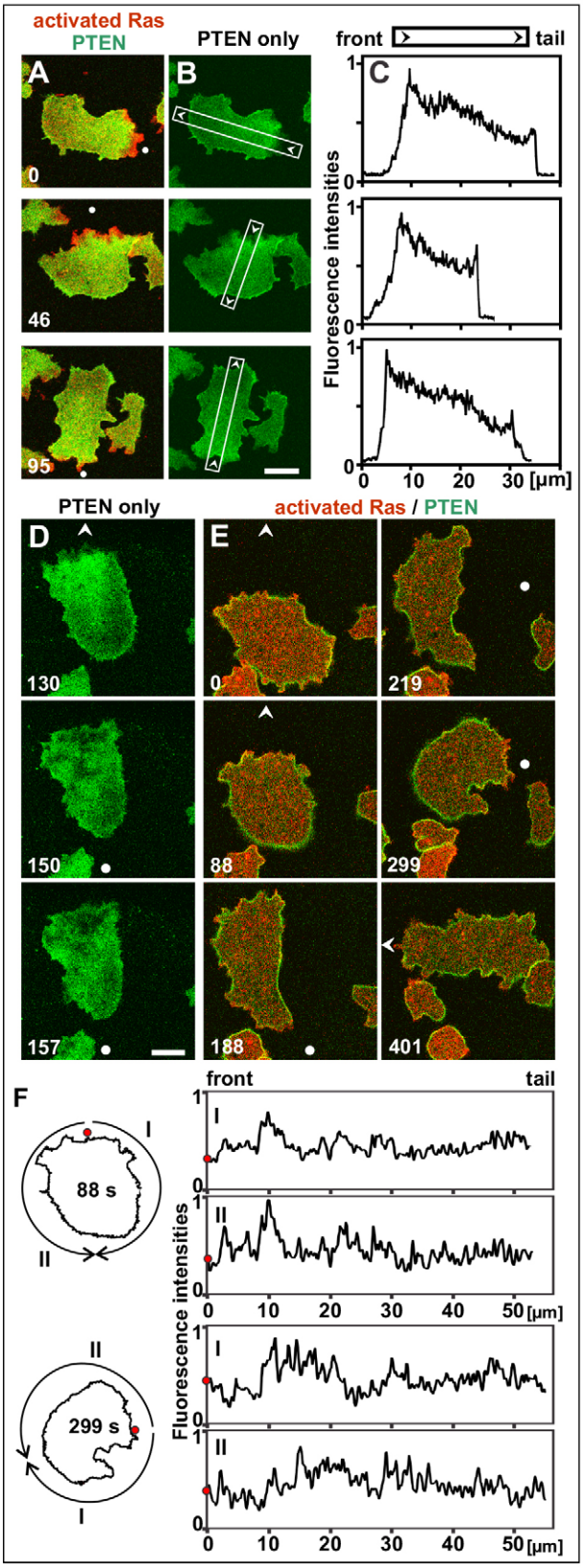

Fig. 6. PTEN patterns within large cells exposed to chemoattractant gradients that repeatedly changed their direction. (A–C) PTEN patterns on the substrate-attached membrane of a reorientating cell. The tip position of the micropipette is indicated by a dot if the tip is located within the frame or by an arrowhead pointing towards a position outside the frame. The 0-s images were acquired at 37 s after the pipette was brought into the position on the right of the frame, the 46-s images at 37 s after the pipette was moved to the top, and the 95-s images at 46 s after the pipette was brought to the bottom. The panels show merged images of activated Ras (red) and PTEN-GFP (green) (A), patterns of PTEN-GFP (B) as used for the scans of fluorescence intensities shown in C. The intensities were scanned along the actual axis of polarity of the cell as indicated by the white bars in B and plotted in arbitrary units. Corresponding arrowheads in B and C indicate the scanning direction. (D,E) Images of a large reorientating cell focused either on the substrate-attached cell surface (D) or 1.5 µm above through the cell body (E). The cell is the same as in Fig. 1B. Time is indicated in seconds after the first frame in E. The 0-s image was acquired at 46 s after the pipette was brought into the position on top of the frame. At 132 s after the 0-s frame the pipette was moved to the bottom, at 201 s to the right, and at 341 s to the left. (F) Scans of fluorescence intensities of PTEN-GFP along the perimeter of the polarised cell at the stages shown in the 88-s and 299-s frames of E. Starting point of the scans is the position closest to the stimulating micropipette (red dot in the diagrams on the left). From this point on, the cell perimeter was scanned up to the tail in clockwise (I) or anti-clockwise direction (II). Scale bars: 10 µm. The entire sequence is shown in Movie 8.

each other. The first phase of reorientation led to two fronts connected by a tail region (330-s frame). At the end, one half of the cell reverted polarity by the emergence of a new front that redirected the actin flow towards the proximal part of the cell (460-s to 476-s frames of Fig. 7C). Strong accumulation of the talC63 fragment resulted in a rounded cluster at the tail of the cell. During chemotactic reorientation, such clusters can be seen to glide along the cortex of the moving cell towards the new tail, suggesting that they are carried by the actin flow (one of these clusters is seen in Movie 11, 239-s to 343-s frames). Taken together, these examples indicate that an actin flow can connect the front (or multiple fronts) with the tail of a large cell, and changes in the direction of an attractant gradient can redirect the actin flow.

DISCUSSION

Reorientation of large cells

In *Dictyostelium* cells that move along a gradient of increasing chemoattractant, the axis of polarity coincides with the direction of the gradient, i.e. the front of the cell pointing towards the source of attractant and the tail in the opposite direction. When the gradient is suddenly reversed, the front of the cell still points into the direction of the previous gradient, such that the attractant hits preferentially the tail region of the cell. The question we addressed here is how cells of increased size respond in this conflict.

The strategies of reorientation in a reversed gradient of chemoattractant varied between two extremes. When the new direction of the gradient determined the response, the cell changed polarity by converting the previous tail into a front. Even very large cells are capable of immediately adjusting their polarity according to changing gradient directions and to orientate with remarkable precision (Fig. 1B). However, when the polarity of a large cell dominated the response, protrusions were induced at the established front, this means at the site of lowest attractant concentration (Fig. 2B and C). Most informative are cases in which one type of behaviour followed the other, as in the cell shown in Movie 2.

A point to emphasize is the highly variable period of time that large cells require to reorientate. Protrusions decorated with activated Ras may be induced at the previous tail region of the cell within 15 s of reverting the direction of the gradient, as shown in Movie 3. But other cells need much longer until a new front is established, which dominates then the movement of the entire cell. This is particularly evident in Movie 2, where the cell started to retract its tail rather than to projecting it towards the source of

Journal of Cell Science (2016) 129, 3462-3472 doi:10.1242/jcs.191148

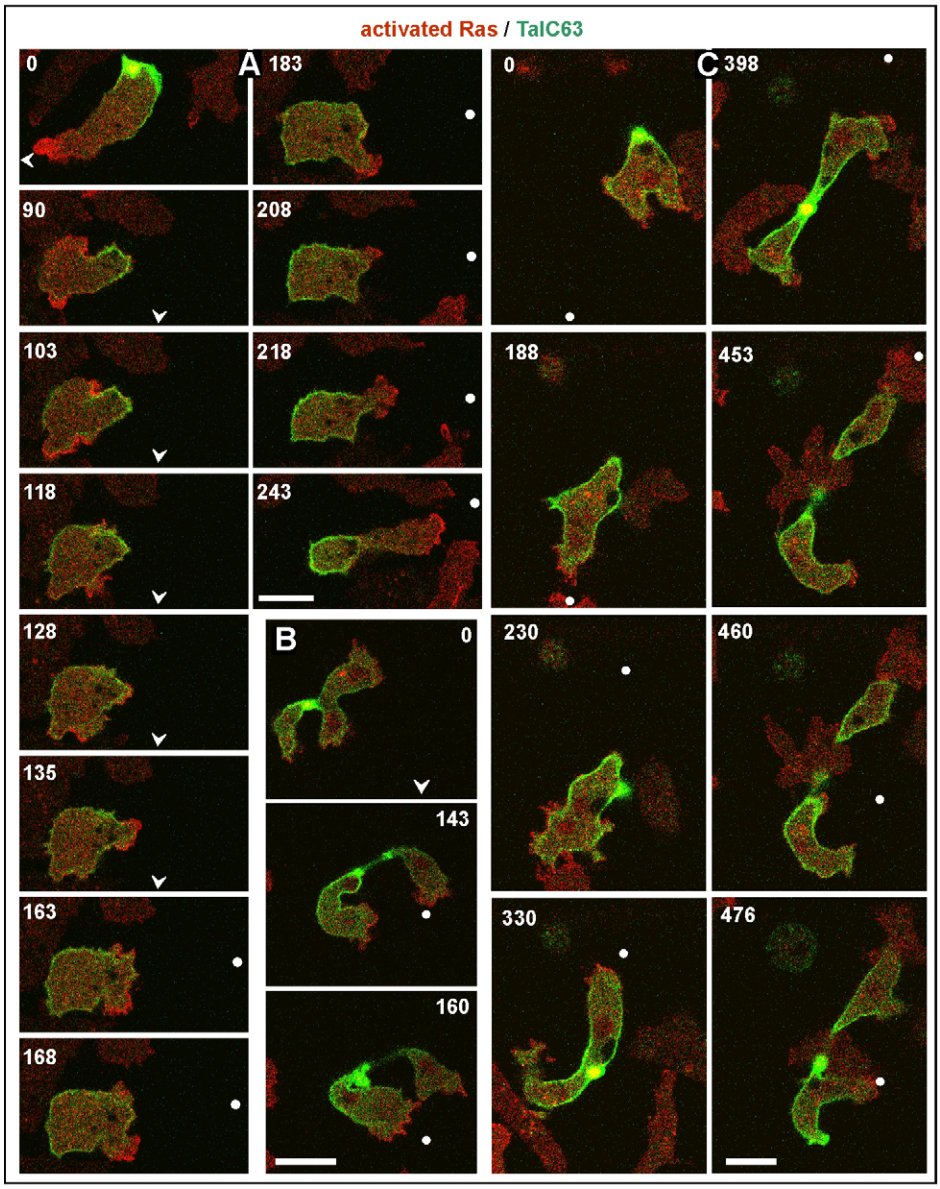

Fig. 7. Redirection of actin flow in changing gradients of attractant. Large cells expressing mRFP-RBD (red) and GFP-talC63 (green).The tip position of the micropipette is indicated by a dot if the tip is located within the frame or by an arrowhead pointing towards a position outside the frame. (A) A cell reverting polarity after changing micropipette position twice. Finally, the actin flow is directed to the previous front. (B) Response with two fronts showing actin flow directed to the junction between the two portions of the cell. (C) Complicated response composed of the types of behaviour shown in A and B. Upon positioning the micropipette to the top of the image, the cell responded by forming two fronts, one close to the source of attractant, the other emerging from the opposite end of the cell. Consequently the actin flow was directed to the middle of the cell. After placing the micropipette to the right, both the upper and lower part of the cell turned into the new direction by forming a new front. Redirection of the actin flow is evident in the lower part. The two halves of the cell remain connected up to the end of the sequence; although this is obscured by the approach of a third cell. For the 476-s frame, the plane of focus has been changed. Numbers indicate seconds after the first frame of each series. Scale bars: 10 µm. The cells are also shown in Movies 9–11.

attractant. Simultaneously, short-lived protrusions appeared at multiple sites of the cell surface. Two of these protrusions persisted, the lateral one turning into the direction of the gradient.

Large cells tended to form multiple protrusions that competed with each other (as in normal-sized cells), but often co-existed for extended periods of time and responded independently to chemoattractant (Fig. 3A and Movie 6). Nevertheless, the large cells eventually succeeded in coordinating protrusion at the new front and retraction at the tail. Even fused cells with a length of 45 µm proved to be capable of coordinating front and tail activities, such that they moved with a defined front pointing to the source of attractant and a tail pointing in the opposite direction (Movie 8).

The display of gain and loss of area in large cells moving in a gradient enables one to identify local activities that are not reliably reflected in the displacement of the centroid of a cell – which is routinely used to calculate the velocity or the chemotactic index as a measure of orientation. An evident discrepancy between local activities and centroid displacement is illustrated in the 8.6-s to 51.6-s frames of Fig. 3C,I. As shown here, the cell formed protrusions beginning in the previous front region when the gradient is reversed but its previous tail retracted in a direction opposite to the new gradient, causing the chemotactic index to become negative.

A local response – the turning of protrusions

Because of the extended periods of independently responding protrusions, the large cells were well-suited to study local responses in chemotaxing cells. The protrusions shown in Fig. 2A–C have cross-sections of 2–4 µm in the direction of the gradient. Turning of these protrusions requires an asymmetry across their diameter, and the activation of Ras on one side of these protrusions reveals the existence of such an asymmetry. This asymmetry argues for a bistable system that creates a plus–minus pattern of Ras activation in the membrane within a cross-section of ~3 µm. To generate this pattern, a localised inhibitory mechanism induced by cAMP may be involved (Xu et al., 2007). The asymmetry is likely to be generated by a spatial rather than a temporal sensing mechanism because protrusions become asymmetric even when they extend tangentially with respect to the gradient (Fig. 2A).

The responses of large cells underscore that protrusions can act as separate response units that independently sense the attractant

Journal of Cell Science (2016) 129, 3462-3472 doi:10.1242/jcs.191148

gradient at different ranges of concentration according to their position along the cell surface. For the turning response, the cell does not need to sense concentration differences over its entire length but only locally over the cross-section of the protrusion. This local response is in accord with a pseudopod-centered model of chemotaxis (Insall, 2010) and is consistent with the view that there are independent spatial signalling domains, each coupled to local pseudopod extension (Arrieumerlou and Meyer, 2005).

Gradient sensing with no requirement for a global inhibitor has been proposed for the chemotropic response to a gradient of α-factor in budding yeast (Hegemann et al., 2015). In this case, the polarity of the cell is established independently of the gradient direction. In a second step, the polarity is aligned with the gradient by local sensing, permitting biased movement of a polarity site along the membrane towards higher density of activated receptors. It has been argued that bacteria cannot sense concentration differences of attractant along their surface because they are too small, whereas bigger eukaryotic cells have a 'spatial awareness' that allows them to sense gradients. In this context, however, note that the cross-section of turning protrusions is similar in size to an *E. coli* cell.

Gradient-independent front-to-tail differentiation

To move in one direction, cells need a global mechanism to coordinate local protrusion and retraction, such that finally a unidirectional front–tail polarity is established. For two models of eukaryotic chemotaxis – i.e. the Gierer–Meinhardt model of short-range activation and long-range inhibition (Meinhardt, 1999), and the LEGI model of local excitation and global inhibition (Levchenko and Iglesias, 2002) – inhibition of front formation along the axis of a polarised cell has been attributed to a diffusible inhibitor. In the Turing-type reaction–diffusion system proposed by Meinhardt and Gierer (2000), the local production of a short-range activator is accompanied by the production of a long-range inhibitor. At the core of the LEGI model is a global mechanism that inhibits the protrusion of a cell front depending on the position in a gradient of chemoattractant (Devreotes and Janetopoulos, 2003). According to this model, all receptors activated on the cell surface by the chemoattractant contribute to an inhibitory signal that equilibrates throughout the entire cell by diffusion. The formation of a protrusion depends on where the local activation exceeds the global inhibition (Iglesias and Devreotes, 2008).

There are three aspects in the chemotactic responses of large cells that need consideration in terms of modelling. First, if the established polarity of the cell dominates, a response is first induced at the established front, arguing for the absence of a global inhibition at this site of lowest attractant concentration. However, the chemotactic response is inhibited at the most-stimulated tail region as opposed to the least-stimulated front region of the cell. We find the turning response at positions far from the source of attractant hard to reconcile with the LEGI mechanism, i.e. with a response on the basis of incremental local activation over global inhibition. Second, the LEGI model is applicable only to cases where inhibition acts along the gradient into the direction of lower chemoattractant concentrations. However, in large cells the inhibition often works perpendicular to the gradient or even in a reverse direction (Fig. 2C and Movie 5). Third, according to the LEGI model, the activation of protrusion by chemoattractant is distinguished as a fast process from that of slow inhibition (Iglesias and Devreotes, 2008; Kutscher et al., 2004). When the large cells had to coordinate the activities of multiple pseudopods, this temporal order of activation and inhibition was disturbed. For instance, the cell in Fig. 2C formed first a protrusion at the established front (15-s frame), this protrusion was subsequently retracted and, simultaneously, another protrusion was formed (46-s frame) that became the new leading edge (58-s to 98-s frames). In the cell of Fig. 2A, retraction of the previous front was a fast response (25-s frame) and establishment of a new front proceeded afterwards (31-s to 70-s frames). As shown in Movie 2, it may take as long as 97 s until a protrusion in the previous tail region is induced.

The distribution of PTEN on the substrate-attached and the free cell surface

The question of how an increased size of the chemotactic response system is reflected in the establishment of polarity was addressed by the recording of activated Ras and membrane-bound PTEN during reorientation. According to data based on normal-sized cells, these markers are distributed along the axis of polarity, with Ras activated at the front and PTEN, being depleted from the front, increasing towards the tail of the cell (Funamoto et al., 2002; Iijima and Devreotes, 2002). These data suggest that PTEN is responsible for restricting PIP3 to the cell front by producing an increasing gradient of PIP3 hydrolysis from the front to the tail. To examine whether this is also true in large cells, the patterns of membrane-bound PTEN during chemotaxis and reorientation were explored.

At the substrate-attached membrane of the large cells, the PTEN distribution was unexpected in that it increased just behind the front and decreased then towards the posterior part of the cell (Fig. 6A–C). This means, at the substrate-attached membrane, the increase of PTEN towards the tail of the cell has a size limit. Thus, the retracting tail of a large cell is distinguished by a low rather than a high decoration with PTEN at its substrate-attached membrane.

The fact that the binding of PTEN to the substrate-attached membrane is restricted to a zone behind the front, is underscored by the regulation of PTEN binding upon the reorientation of a cell. When the anterior region of the cell is converted into a posterior region, membrane-bound PTEN is downregulated characteristically by local detachment producing 'PTEN holes' at the membrane (Fig. 6D; Movie 8). These PTEN-depleted patches increase in size until they fuse into a uniformly depleted area. This mode of downregulation has previously been found in the context of actin wave formation (Gerisch et al., 2012) and has been modelled by Knoch et al. (2014).

In cross-sections through large cells at 1.5 µm above their substrate-attached surface, the front proved to be sub-divided into clusters of activated Ras where protrusion occurs, indicating that the external gradient is not uniformly translated into a front-to-tail pattern at the membrane of the cells (Fig. 6E). This clustering is consistent with the patch formation of activated Ras and PIP3 in chemoattractant-stimulated cells of normal size (Hecht et al., 2011; Postma et al., 2004; Xiong et al., 2010). PTEN was more uniformly distributed in the tail region, but not generally enriched there relative to the front (Fig. 6F). It, therefore, seems unlikely that a PTEN gradient is responsible for polarity of the large cells. This notion is in accordance with the finding that PIP3, the substrate of this PI3-phosphatase, is not essential for the chemotactic responsiveness of *Dictyostelium* cells (Hoeller and Kay, 2007).

A global actin flow connects the front and tail of a chemotaxing cell

A remaining question is whether there are mechanisms other than diffusion that might transmit an inhibitory signal from an established front to the tail of a cell. One possibility is the inhibition of pseudopod formation by the increase of membrane

Journal of Cell Science (2016) 129, 3462-3472 doi:10.1242/jcs.191148

tension caused by a local protrusion, as explored for neutrophil polarity by Houk et al. (2012) and reviewed by Sens and Plastino (2015). Another possibility is the retrograde transport of an inhibitor along the cell cortex. The polarity of a migrating *Dictyostelium* cell is reflected in the direction of an actin flow (Lee et al., 1998). This flow is a way of communication between the front and tail regions of a cell; it can be visualised by a reporter construct, GFP-tagged C63, based on an actin-binding domain of talin (Weber et al., 2002). As demonstrated by this reporter, a signalling molecule transported by a directed flow will accumulate at the tail of the cell, which is distinct from diffusion that would result only in a uniform concentration. In mammalian cells, the maintenance of cell polarity is coupled by a positive-feedback loop to the velocity of an actin flow that transports polarisation cues, and thus causes an asymmetry of their distribution depending on their affinity to actin (Maiuri et al., 2015).

We used the talin C63 probe to demonstrate that large cells produced by electric-pulse-induced fusion can establish a monotonic front–tail polarity, and either turn or reverse this polarity when they respond to changing directions of a gradient. The flow reporter accumulated at the actual tail region of a large cell (Fig. 7A), even when this region was located in the middle between two or three fronts (Fig. 7B). The induction of a new front redirected the flow, as shown in the 453-s to 476-s frames of Fig. 7C. Thus, to account for global inhibition in a chemotaxing cell, one might assume that there is an inhibitor that is linked to filamentous actin and is transported in a similar manner to the reporter used here. In accordance with the removal of a protrusion inhibitor from the front of cells that respond to a reversed gradient, the established front remained sensitive to attractant and only the tail became desensitised until the polarity was reversed (Movie 2).

Conclusions

The chemotactic responses of eukaryotic cells can be conceptually divided into four stages: (1) induction of protrusions, (2) turning of these protrusions into the direction of the gradient, (3) competition between the protrusions and, (4) global redirection of cell polarity.

(1) When the gradient of chemoattractant is reversed, protrusions can be induced at several sites along the front-to-tail axis of large cells. If the induction has a bias towards the intrinsic polarity of the cell, protrusions are preferentially induced at the established front of the cell, i.e. at sites of lowest attractant concentration. If the gradient is strong enough to override the polarity, the protrusions will be induced at sites of highest attractant concentration, i.e. at the previous tail of the cell. Details of the chemotactic responses of large cells are revealed by displaying gain and loss of cell area. These responses are not necessarily represented in the displacement of the centroid of the cell and are, therefore, not reflected in the chemotactic index based on this displacement.

(2) Irrespective of the site of their origin, growing protrusions tend to turn into the direction of the gradient. Asymmetric Ras activation in turning protrusions is an argument for a localised mechanism of gradient sensing.

(3) Multiple protrusions on the surface of a large cell compete with each other. The inhibition does not necessarily act in the direction of lower attractant concentration, suggesting a mechanism that is independent of the attractant gradient.

(4) Redirection of polarity is coupled to redirection of a global actin flow. The latter can transport actin-binding proteins from the front of a chemotaxing cell to its tail, where they accumulate reversible manner.

MATERIALS AND METHODS

Cell culture and strains

Transformants expressing fluorescent proteins were derived from the AX2-214 strain of *D. discoideum* and cultivated in nutrient medium containing 10 µg/ml of blasticidin (Invitrogen, Life Technologies, Grand Island, NY) and 10 µg/ml of G418 (Sigma-Aldrich, St Louis, MO). For the expression of PTEN-sfGFP, the full-length genomic sequence of *D. discoideum* PTEN (DDBG0286557) was cloned into the *Eco*RI-site of a pDEX-based expression vector in frame with superfolder GFP (Pedelacq et al., 2006) as described by Müller-Taubenberger and Ishikawa-Ankerhold (2013). Transformants were selected by using 20 µg/ml of G418.

For the mRFP-Raf1-RBD construct, the minimal Ras-binding domain (RBD) of human Raf proto-oncogene serine/threonine-protein kinase (Raf-1) was employed as an activation-specific probe for Ras (de Rooij and Bos, 1997; Nassar et al., 1995). A gene fragment comprising amino-acid residues 55-131 was synthesised, with the nucleotide sequence adapted to the *Dictyostelium* codon usage (Eurofins MWG Operon), and cloned via *Bam*HI and *Eco*RI into a pDEX-based mRFP-expression vector (Müller-Taubenberger, 2006). Double-transformants were selected by using 10 µg/ml of blasticidin and 20 µg/ml of G418. To monitor the actin flow, a strain that expressed a GFP-tagged C-terminal 63-kDa fragment of talin A from *D. discoideum* was used (Weber et al., 2002). Cells were cultivated and imaged at 21±2°C.

Cell fusion

Cells from six sub-confluent Petri dishes were harvested in 60 ml of 17-mM K/Na-phosphate buffer pH 6.0, washed with 20 ml buffer, adjusted to 1.5×10^7 cells/ml and gently shaken for 5 h in a roller tube, allowing the cells to agglutinate (Gerhardt et al., 2014). By using a pipette with the tip cut-off to prevent dissociation, aliquots of the suspension were transferred to electroporation cuvettes with an electrode distance of 4 mm and fused in a BioRad Gene Pulser Model 1652077 (Bio-Rad Laboratories, Hercules, CA) by applying three pulses of 1 kV at 1-s intervals. A 20-µl aliquot of the fused cell suspension was transferred into a tissue-culture dish with a glass coverslip bottom (FluoroDish, WPI, Inc., Sarasota, FL). After 5 min, 3 ml of the phosphate buffer supplemented with 2 mM $CaCl_2$ and 2 mM $MgCl_2$ were added, and after settling the cells were subjected to imaging.

Chemotactic stimulation and image analysis

For chemotactic stimulation, a Femtotip® microcapillary (Eppendorf, Köln, Germany) was filled with 10^{-4} M cAMP solution and connected to a micromanipulator (Micro Control Instruments Ltd., East Sussex, UK). The pipette tip was lowered until it had reached the field of view and was then moved into the vicinity of a cell.

Confocal images were acquired with a Zeiss LSM 780 equipped with a Plan-Apo 63x/NA 1.46 oil immersion objective (Carl Zeiss Microscopy, Jena, Germany), and analysed using the image processing package Fiji (http://Fiji.sc/Fiji) developed by Schindelin et al. (2012) on the basis of ImageJ (http://imagej.nih.gov/ij).

To display gain and loss of cell area, cells expressing mRFP-RBD and PTEN-GFP were recorded at the substrate-attached surface and 1.5 µm beyond that surface. The two images were superimposed and the combined images used to determine the cell perimeter and centroid. Centroids were located by using the ROI tool of Fiji. Positions of centroids and pipet tips were plotted as an image sequence in Fiji, and with the MTrackJ tool the tracks between centroid to centroid and centroid to pipet position were identified and pasted in an Excel sheet. The angles of the tracks were used to gain the angle α between the tracks, and the chemotactic index was calculated by taking the cosine of α. Velocities of centroid displacement and the chemotactic indices were plotted against the time in Excel.

Acknowledgements

We thank Martin Spitaler and his staff for providing imaging facilities, and Petra Fey and dictyBase for informations.

Competing interests

The authors declare no competing or financial interests.

Author contributions

M.L. performed experiments and evaluated the results, J.P. and M.E. analysed data, and A.M.-T. made the fluorescent protein constructs. G.G. designed the research project and wrote the paper.

Funding

G.G. thanks the Max-Planck-Gesellschaft for support; and A.M.-T. the Deutsche Forschungsgemeinschaft for grants to the SFB 914, TP7.

Supplementary information

Supplementary information available online at
http://jcs.biologists.org/lookup/doi/10.1242/jcs.191148.supplemental

References

Andrew, N. and Insall, R. H. (2007). Chemotaxis in shallow gradients is mediated independently of PtdIns 3-kinase by biased choices between random protrusions. *Nat. Cell Biol.* **9**, 193-200.

Arai, Y., Shibata, T., Matsuoka, S., Sato, M. J., Yanagida, T. and Ueda, M. (2010). Self-organization of the phosphatidylinositol lipids signaling system for random cell migration. *Proc. Natl. Acad. Sci. USA* **107**, 12399-12404.

Arrieumerlou, C. and Meyer, T. (2005). A local coupling model and compass parameter for eukaryotic chemotaxis. *Dev. Cell* **8**, 215-227.

Bosgraaf, L. and Van Haastert, P. J. (2009). The ordered extension of pseudopodia by amoeboid cells in the absence of external cues. *PLoS ONE* **4**, e5253.

de Rooij, J. and Bos, J. L. (1997). Minimal Ras-binding domain of Raf1 can be used as an activation-specific probe for Ras. *Oncogene* **14**, 623-625.

Devreotes, P. and Janetopoulos, C. (2003). Eukaryotic chemotaxis: distinctions between directional sensing and polarization. *J. Biol. Chem.* **278**, 20445-20448.

Funamoto, S., Meili, R., Lee, S., Parry, L. and Firtel, R. A. (2002). Spatial and temporal regulation of 3-phosphoinositides by PI 3-kinase and PTEN mediates chemotaxis. *Cell* **109**, 611-623.

Gerhardt, M., Ecke, M., Walz, M., Stengl, A., Beta, C. and Gerisch, G. (2014). Actin and PIP3 waves in giant cells reveal the inherent length scale of an excited state. *J. Cell Sci.* **127**, 4507-4517.

Gerisch, G., Schroth-Diez, B., Müller-Taubenberger, A. and Ecke, M. (2012). PIP3 waves and PTEN dynamics in the emergence of cell polarity. *Biophys. J.* **103**, 1170-1178.

Gerisch, G., Ecke, M., Neujahr, R., Prassler, J., Stengl, A., Hoffmann, M., Schwarz, U. S. and Neumann, E. (2013). Membrane and actin reorganization in electropulse-induced cell fusion. *J. Cell Sci.* **126**, 2069-2078.

Hecht, I., Skoge, M. L., Charest, P. G., Ben-Jacob, E., Firtel, R. A., Loomis, W. F., Levine, H. and Rappel, W. J. (2011). Activated membrane patches guide chemotactic cell motility. *PLoS Comput. Biol.* **7**, e1002044.

Hegemann, B., Unger, M., Lee, S. S., Stoffel-Studer, I., van den Heuvel, J., Pelet, S., Koeppl, H. and Peter, M. (2015). A cellular system for spatial signal decoding in chemical gradients. *Dev. Cell* **35**, 458-470.

Hoeller, O. and Kay, R. R. (2007). Chemotaxis in the absence of PIP3 gradients. *Curr. Biol.* **17**, 813-817.

Huang, C.-H., Tang, M., Shi, C. J., Iglesias, P. A. and Devreotes, P. N. (2013). An excitable signal integrator couples to an idling cytoskeletal oscillator to drive cell migration. *Nat. Cell Biol.* **15**, 1307-1316.

Houk, Andrew R., Jilkine, A., Mejean, Cecile O., Boltyanskiy, R., Dufresne, Eric R., Angenent, Sigurd B., Altschuler, Steven J., Wu, Lani F. and Weiner, Orion D. (2012). Membrane Tension Maintains Cell Polarity by Confining Signals to the Leading Edge during Neutrophil Migration. *Cell* **148**, 175-188.

Iglesias, P. A. and Devreotes, P. N. (2008). Navigating through models of chemotaxis. *Curr. Opin Cell Biol.* **20**, 35-40.

Iijima, M. and Devreotes, P. (2002). Tumor suppressor PTEN mediates sensing of chemoattractant gradients. *Cell* **109**, 599-610.

Insall, R. H. (2010). Understanding eukaryotic chemotaxis: a pseudopod-centred view. *Nat. Rev. Mol. Cell Biol.* **11**, 453-458.

Kae, H., Kortholt, A., Rehmann, H., Insall, R. H., Van Haastert, P. J., Spiegelman, G. B. and Weeks, G. (2007). Cyclic AMP signalling in Dictyostelium: g-proteins activate separate Ras pathways using specific RasGEFs. *EMBO Rep.* **8**, 477-482.

Knoch, F., Tarantola, M., Bodenschatz, E. and Rappel, W. J. (2014). Modeling self-organized spatio-temporal patterns of PIP3 and PTEN during spontaneous cell polarization. *Phys. Biol.* **11**, 046002.

Kutscher, B., Devreotes, P. and Iglesias, P. A. (2004). Local excitation, global inhibition mechanism for gradient sensing: an interactive applet. *Sci. Signal.* **2004**, pl3-pl3.

Lee, E., Shelden, E. A. and Knecht, D. A. (1998). Formation of F-actin aggregates in cells treated with actin stabilizing drugs. *Cell Motil. Cytoskeleton* **39**, 122-133.

Levchenko, A. and Iglesias, P. A. (2002). Models of eukaryotic gradient sensing: application to chemotaxis of amoebae and neutrophils. *Biophys. J.* **82**, 50-63.

Maiuri, P., Rupprecht, J.-F., Wieser, S., Ruprecht, V., Bénichou, O., Carpi, N., Coppey, M., De Beco, S., Gov, N., Heisenberg, C. P. et al. (2015). Actin flows mediate a universal coupling between cell speed and cell persistence. *Cell* **161**, 374-386.

Meinhardt, H. (1999). Orientation of chemotactic cells and growth cones: models and mechanisms. *J. Cell Sci.* **112**, 2867-2874.

Meinhardt, H. and Gierer, A. (2000). Pattern formation by local self-activation and lateral inhibition. *BioEssays* **22**, 753-760.

Müller-Taubenberger, A. (2006). Application of fluorescent protein tags as reporters in live-cell imaging studies. *Methods Mol. Biol.* **346**, 229-246.

Müller-Taubenberger, A. and Ishikawa-Ankerhold, H. C. (2013). Fluorescent reporters and methods to analyze fluorescent signals. *Methods Mol Biol* **983**, 93-112.

Nassar, N., Horn, G., Herrmann, C. A., Scherer, A., McCormick, F. and Wittinghofer, A. (1995). The 2.2 A crystal structure of the Ras-binding domain of the serine/threonine kinase c-Raf1 in complex with Rap1A and a GTP analogue. *Nature* **375**, 554-560.

Pédelacq, J. D., Cabantous, S., Tran, T., Terwilliger, T. C. and Waldo, G. S. (2006). Engineering and characterization of a superfolder green fluorescent protein. *Nat. Biotechnol.* **24**, 79-88.

Postma, M., Roelofs, J., Goedhart, J., Loovers, H. M., Visser, A. J. and Van Haastert, P. J. (2004). Sensitization of Dictyostelium chemotaxis by phosphoinositide-3-kinase-mediated self-organizing signalling patches. *J. Cell Sci.* **117**, 2925-2935.

Takeda, K., Shao, D., Adler, M., Charest, P. G., Loomis, W. F., Levine, H., Groisman, A., Rappel, W.-J. and Firtel, R. A. (2012). Incoherent feedforward control governs adaptation of activated ras in a eukaryotic chemotaxis pathway. *Sci. Signal.* **5**, ra2.

Schindelin, J., Arganda-Carreras, I., Frise, E., Kaynig, V., Longair, M., Pietzsch, T., Preibisch, S., Rueden, C., Saalfeld, S. and Schmid, B. (2012). Fiji: an open-source platform for biological-image analysis. *Nat. Methods* **9**, 676-682.

Sens, P. and Plastino, J. (2015). Membrane tension and cytoskeleton organization in cell motility. *J. Phys. Condens. Matter* **27**, 273103.

Weber, I., Niewöhner, J., Du, A., Röhrig, U. and Gerisch, G. (2002). A talin fragment as an actin trap visualizing actin flow in chemotaxis, endocytosis, and cytokinesis. *Cell Motil. Cytoskeleton* **53**, 136-149.

Xiong, Y., Huang, C.-H., Iglesias, P. A. and Devreotes, P. N. (2010). Cells navigate with a local-excitation, global-inhibition-biased excitable network. *Proc. Natl. Acad. Sci. USA* **107**, 17079-17086.

Xu, X., Meier-Schellersheim, M., Yan, J. and Jin, T. (2007). Locally controlled inhibitory mechanisms are involved in eukaryotic GPCR-mediated chemosensing. *J. Cell Biol.* **178**, 141-153.

Zhang, S., Charest, P. G. and Firtel, R. A. (2008). Spatiotemporal regulation of Ras activity provides directional sensing. *Curr. Biol.* **18**, 1587-1593.

Supplementary Information

Movies

All movies show enlarged cells obtained by electric-pulse induced fusion. Tip positions of a micropipette filled with cyclic AMP are indicated by dots or arrowheads as in the figures. Seconds after the first frame of each sequence are indicated. The scale bars in the first frames indicate 10 µm.

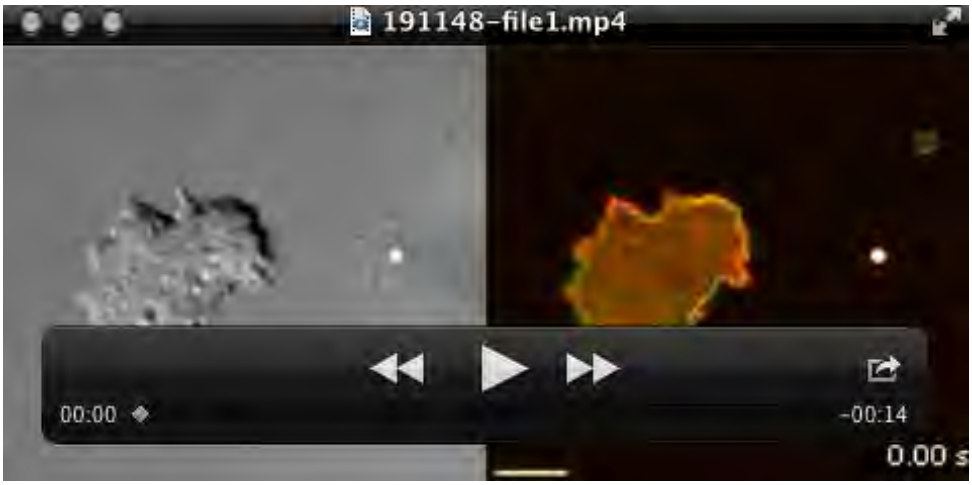

Movie 1. **Three cells of different sizes responding to changing positions of a micropipette filled with the chemoattractant.** The cells are labeled for activated Ras (red) and express GFP-PTEN (green). The left panels display bright-field DIC images, the right panels confocal cross-sections though the cell at a plane 1.5 µm beyond the substrate surface. The middle cell exemplifies that large cells may respond almost as fast as small ones: when the micropipette is moved from the right to the left at 235.44 s and 514.08 s, the first protrusions with activated Ras which are formed at the previous tail become detectable at 252.72 s and 529.20 s, respectively. In particular the large cell entering from top responds with a broad front, which is sub-divided into sections occupied with activated Ras and interspersed with PTEN-decorated zones. The same cells are shown in Figure 1A; the 170-s image of the Movie corresponding to the 0-s frame in the Figure. Frame-to-frame interval 2.16 s.

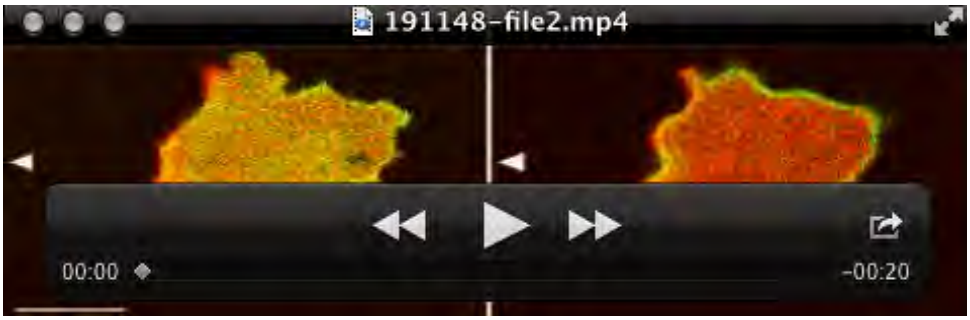

Movie 2. **Merged confocal images of a large cell labeled for activated Ras (red) and expressing PTEN-GFP (green).** The left panels are focused on the substrate-attached cell surface, the right panels display cross-sections through the cell bodies at a plane 1.5 µm beyond the substrate-attached surface. The cell re-orientates twice, showing various responses to reversal of the attractant gradient. In the periods of the 51.60-s to 94.60-s frames and of the 172.00 to 268.75-s frames the previous tail, now exposed to the source of attractant, retracts rather than protrudes toward the micropipette. In the 174.15-s to 180.60-s period, a thin protrusion emanating at the right border of the frame is seen in the left panel to turn into the direction of the gradient, with activated Ras at its tip. In the 184.90-s to 245.10-s frames, the formation of protrusions progresses at the bottom part of the cell from the previous front (opposite to the actual micropipette position) toward the newly established front. Frame-to-frame interval 2.15 s.

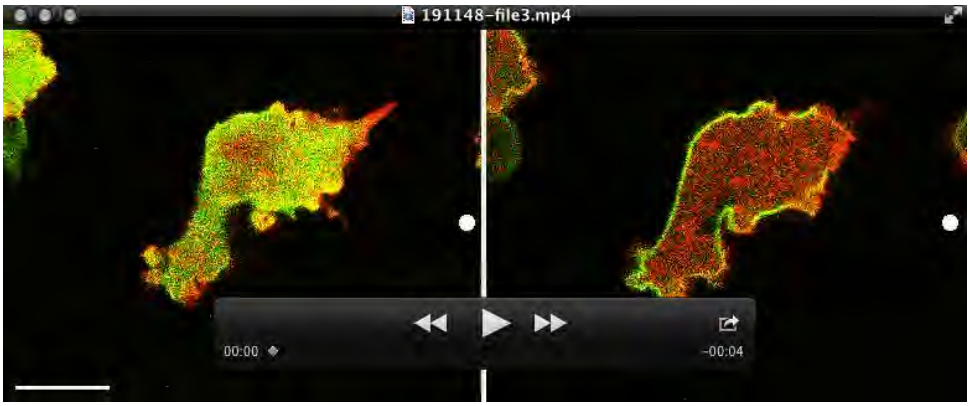

Movie 3. **Recording similar to Movie 2. The same cell is displayed in Figure 2A**; the 9.18-s image corresponding to the 0-s frame in Figure 2A. Frame-to-frame interval 3.06 s.

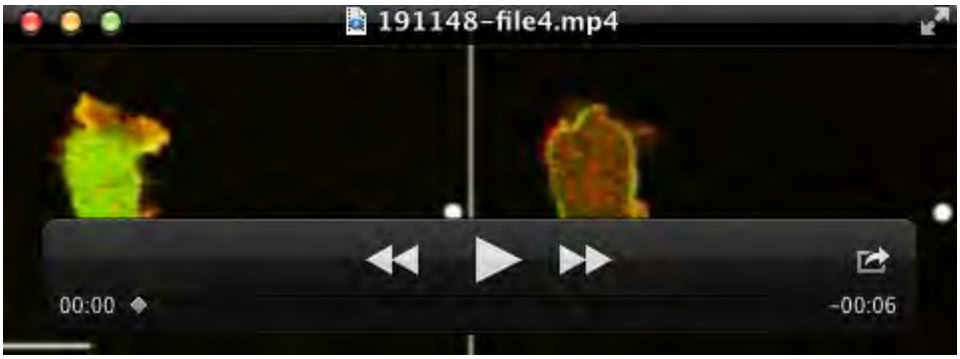

Movie 4. R**ecording similar to Movie 2 of the cell displayed in Figure 2B.** Frame-to-frame interval 3.06 s. The 15.30-s image corresponds to the 0-s frame in Figure 2B.

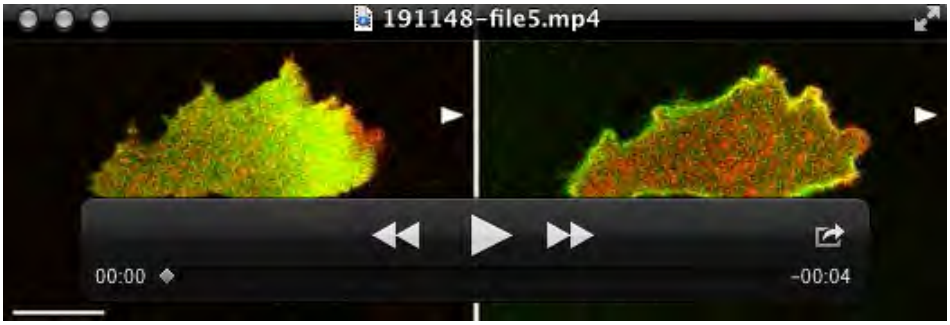

Movie 5. **Recording similar to Movie 2 of the cell displayed in Figure 2C.** Frame-to-frame interval 3.06 s. The 12.24-s image corresponds to the 0-s frame in Figure 2C.

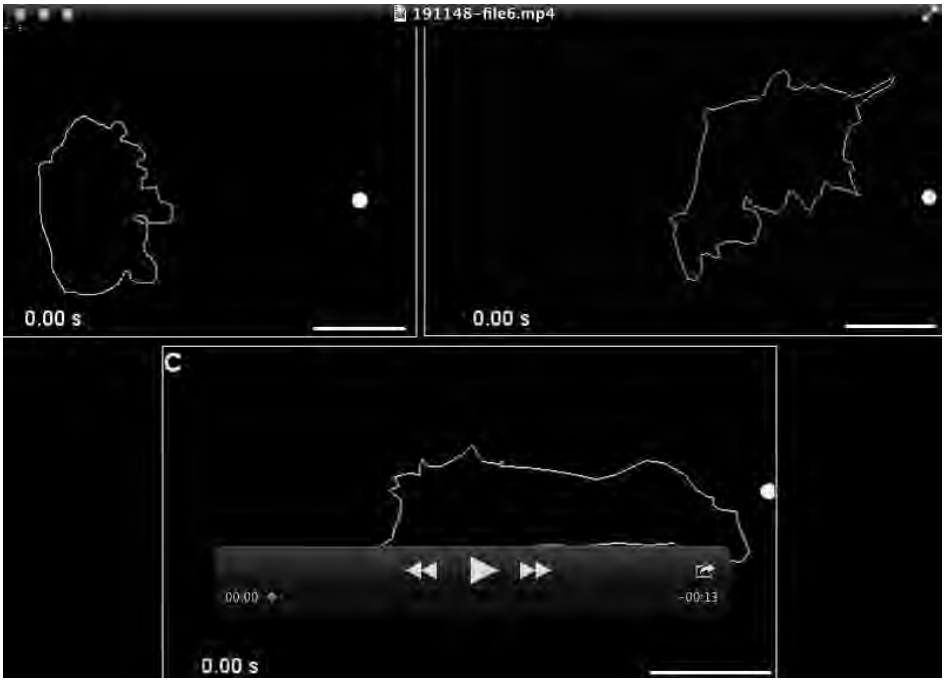

Movie 6. **Gain (red) and loss (blue) of cell area from one frame to the next in three cells responding to reversal of an attractant gradient.** The cells in A, B, and C are the same as in Figure 3A, B, and C. Micropipette positions are indicated by white dots.

Frame-to-frame intervals are for A and B 9.18 s, for C 8.60 s.

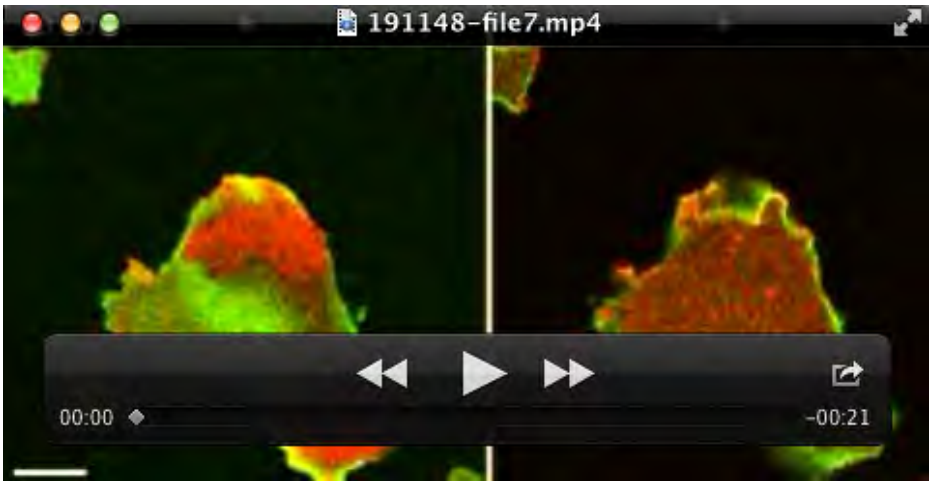

Movie 7. **A very large cell that forms waves on the substrate-attached membrane and responds to gradients of chemoattractant.** The cell recorded similar to Movie 2, forms propagating waves of activated Ras (red) on the substrate-attached membrane and simultaneously responds to changing directions of chemoattractant.

Frame-to-frame interval 2.16 s.

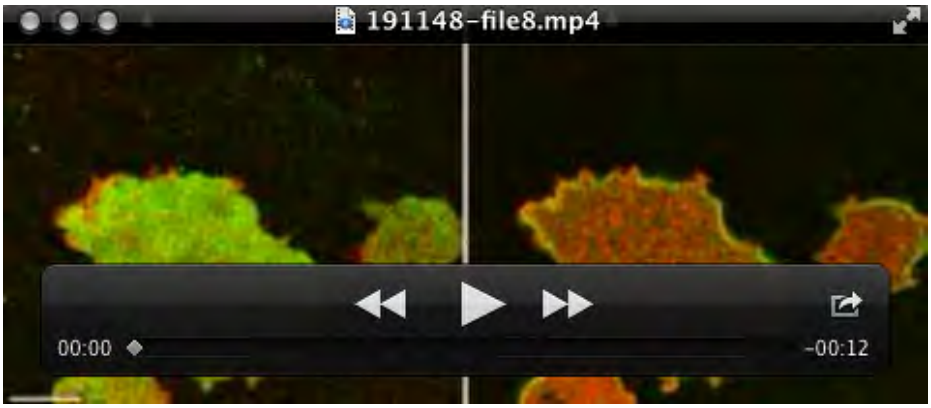

Movie 8. **Recording similar to Movie 2 of the cell displayed in Figures 6D and E.** Frame-to-frame interval 2.09 s. The 0-s image corresponds to the 0-s frame in Figure 6E.

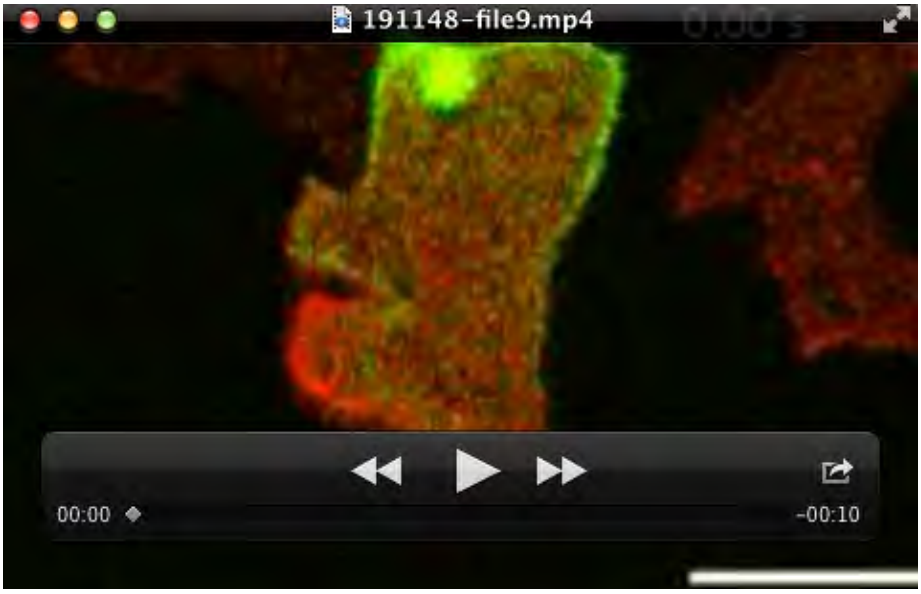

Movie 9. **Confocal section through a cell expressing mRFP-RBD to label activated Ras (red), and GFP-talC63 (green) that accumulates in the direction of actin flow.** The focus is placed 1.5 µm above the substrate surface. The same cell is shown in Figure 7A. Frame-to-frame interval 2.50 s. The 30.00-s image corresponds to the 0-s frame in Figure 7A.

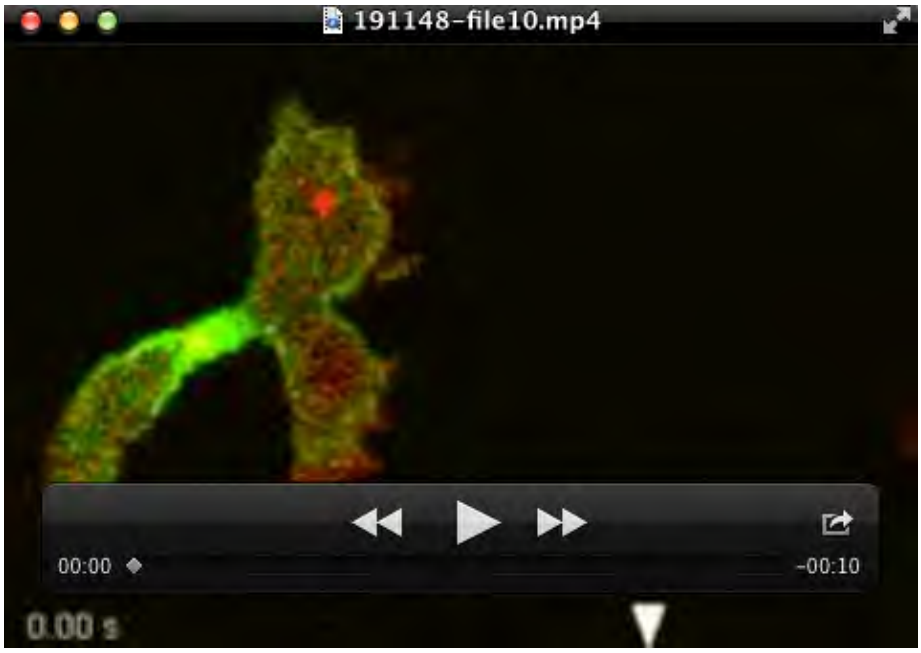

Movie 10. **Recording similar to Movie 9 of the cell displayed in Figure 7B.** Frame-to-frame interval 2.53 s. The 17.71-s image corresponds to the 0-s frame in Figure 7B.

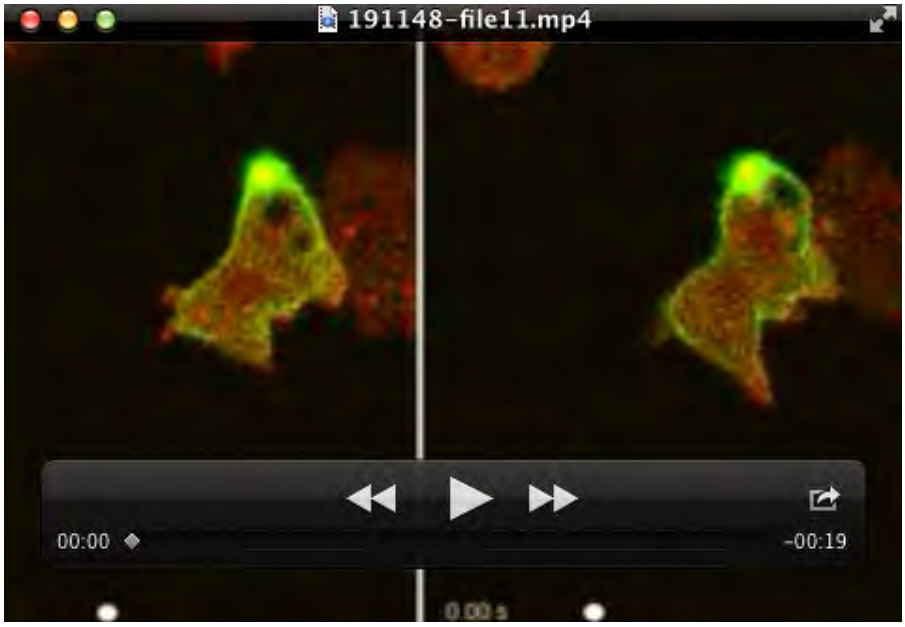

Movie 11. **Recording of the cell displayed in Figure 7C, labeled as in Movie 9.** Left and right panels represent two planes of focus 1.5 µm apart of each other. Frame-to-frame interval 2.54 s. The 15.24-s image corresponds to the 0-s frame in Figure 7C.